Journal of Neuroscience Methods 289 (2017) 75–84

Contents lists available at ScienceDirect

Journal of Neuroscience Methods

journal homepage: www.elsevier.com/locate/jneumeth

A general protocol of ultra-high resolution MR angiography to image the cerebro-vasculature in 6 different rats strains at high field

Géraldine Pastor[a], María Jiménez-González[a,1], Sandra Plaza-García[a], Marta Beraza[a], Daniel Padro[a], Pedro Ramos-Cabrer[a,b,*], Torsten Reese[a,*]

[a] Molecular Imaging Unit, CIC biomaGUNE, Paseo de Miramón 182, 20014 Donostia-San Sebastián, Spain
[b] Ikerbasque, Basque Foundation for Science, 48013 Bilbao, Spain

HIGHLIGHTS

- MR angiography in six different rat strains at high field.
- Robust time-of-flight protocol to image the cerebro-vasculature of the rat.
- Visualization of the hypothalamic and anterior choroidal artery.
- Detection of the posterior inferior cerebellar artery.
- Simple post-processing to aid visualization.

ARTICLE INFO

Article history:
Received 17 March 2017
Received in revised form 6 July 2017
Accepted 6 July 2017
Available online 8 July 2017

Keywords:
High magnetic field
Ischemia models
Magnetic resonance angiography
Maximum intensity projection
Middle cerebral artery occlusion
Post-processing
Rat
Strain dependence
Ultra-high resolution
Visualization

ABSTRACT

Background: Differences in the cerebro-vasculature among strains as well as individual animals might explain variability in animal models and thus, a non-invasive method tailored to image cerebral vessel of interest with high signal to noise ratio is required.
New method: Experimentally, we describe a new general protocol of three-dimensional time-of-flight magnetic resonance angiography to visualize non-invasively the cerebral vasculature in 6 different rat strains. Flow compensated angiograms of Sprague Dawley, Wistar Kyoto, Lister Hooded, Long Evans, Fisher 344 and Spontaneous Hypertensive Rat strains were obtained without the use of contrast agents. At 11.7 T using a repetition time of 60 ms, an isotropic resolution of up to 62 μm was achieved; total imaging time was 98 min for a 3D data set.
Results: The visualization of the cerebral arteries was improved by removing extra-cranial vessels prior to the calculation of maximum intensity projection to obtain the angiograms. Ultimately, we demonstrate that the newly implemented method is also suitable to obtain angiograms following middle cerebral artery occlusion, despite the presence of intense vasogenic edema 24 h after reperfusion.
Comparison with existing methods: The careful selection of the excitation profile and repetition time at a higher static magnetic field allowed an increase in spatial resolution to reliably detect of the hypothalamic artery, the anterior choroidal artery as well as arterial branches of the peri-amygdoidal complex and the optical nerve in six different rat strains.
Conclusions: MR angiography without contrast agent can be utilized to study cerebro-vascular abnormalities in various animal models.

1. Introduction

Studies of cerebral ischemia are hampered by variability in infarct size 24–48 h following middle cerebral artery occlusion (MCAO) (Fox et al., 1993), importantly affecting all strains to various degrees (Sauter and Rudin, 1995; Howells et al., 2010). Hereby, potential differences in the cerebro-vasculature between strains may explain the difference, especially with respect to collateral

* Corresponding author.
E-mail addresses: pramos@cicbiomagune.es (P. Ramos-Cabrer), treese@cicbiomagune.es (T. Reese).
[1] Present address: Metabolism Division, Johns Hopkins University, CMSC Building 10-113, Baltimore, MD, 21287, USA.

http://dx.doi.org/10.1016/j.jneumeth.2017.07.003

flow to areas affected by MCAO. One method to visualize anatomical differences of the cerebro-vasculature between individuals and strains is magnetic resonance angiography (MRA) (Reese et al., 1999). Time-of-flight (TOF) MRA methods rely on the flow related enhancement (FRE) of blood entering into an imaging slab from one end (Bernstein et al., 2004). Stationary signal is successfully suppressed by the use of repetitive excitation, whereby freshly inflowing blood gives rise to increased signal intensity in comparison to stationary signal. Alternatively, ultra-high resolution angiograms of the rat cerebral vasculature were recorded in 7 h 16 min using Gd(DTPA) as an intravascular contrast agent (Mellin et al., 1994).

In theory, MRA can be performed before, in naïve animals, as well as during and/or after MCAO. Generally, when animals arrive at the imaging facility, they could be pre-screened by MRI to evaluate their suitability for experimental stroke models. Hereby, animals with abnormal cerebral arteries or enlarged ventricles, hydrocephalus could be identified and excluded from the study prior to surgery to reduce the variability measure of outcome. During MCAO, a successful occlusion could be visualized by MRA (Dittmar et al., 2006; Besselmann et al., 2001) in parallel with measures that detect a reduction in perfusion in the affected area like arterial spin labeling MRI or laser Doppler flowmetry (Kloiber et al., 1993; Lythgoe et al., 2000; Yushmanov et al., 2002; Bardutzky et al., 2005; Weber et al., 2006; Gao et al., 2014; Cuccione et al., 2016). Likewise, immediately following a transient MCAO, a successful reperfusion might be visualized by MRA and confirmed by perfusion readouts to exclude animals and minimize experimental variability within the study cohort (Reese et al., 1999). As putative treatment regimen might influence cerebral perfusion, a characterization of the MCA branching off from the circle of Willis might be the only direct measure to detect abnormalities in the cerebro-vasculature within a study cohort to justify an inclusion or exclusion of a specific animal. An acquisition of MRAs days or weeks following cerebral ischemia would offer the advantage to be able to schedule the imaging session as an extension of routine experiments required to obtain the infarct size and location by T2-weighted MR. Importantly, as longitudinal MR studies often require multiple imaging sessions, one has to keep in mind that they are labor intensive and expensive with respect to data acquisition and analysis, a focus on animals that will be ultimately included in the study report will be beneficial. The benefit to identify unwanted outliers early will increase with the complexity of the study design, e.g. when behavioral and functional MR and positron emission tomography (PET) studies are interleaved. Thus, generic advantages of the use as well as the disadvantages of MRA in experimental stroke models are briefly discussed.

The purpose of this work is to establish a robust protocol of 3D-time-of-flight (TOF) MRA suitable to image the arterial vasculature of the rat without the use of contrast agents in different strains. Several imaging protocols differing in the required spatial and temporal resolution were utilized to improve upon previously reported protocols (Reese et al., 1999). The methods were then applied to an experimental stroke model of 60 min transient MCAO using an intra-luminal thread (Koizumi et al., 1986; Belayev et al., 1996). The 3D-TOF MR angiograms were obtained in the rat 24 h after re-perfusion, in the same anesthetic session that acquired the T2-weighted images to derive the infarct size.

2. Material and methods

2.1. Animals

All animal procedures had been reported according ARRIVE guidelines and were approved by the ethical committee of CIC biomaGUNE, an AAALAC accredited institution, and local authorities, according to the specific Spanish (RD 53/2013) and European Union (Directive 2010/63/EU) legislation.

2.1.1. Different rat strains

Healthy male rats of six different strains (n = 2 of each strain, 240–345 g) were used in this study. Sprague Dawley (SD), Wistar Kyoto (WK), Spontaneous Hypertensive Rats (SHR) and Long Evans (LE) provided by Janvier Labs (Saint-Berthevin Cedex, France) and Fischer 344 (FI) and Lister Hooded (LH) rats by Charles River Laboratories (Calco, Italy) were allowed to rest in individually ventilated cages, with an enriched environment for animal welfare, for at least five days following transport and had free access to food and water.

2.1.2. Transient ischemia in Sprague Dawley rats

The experimental procedure was performed following criteria derived from the Stroke Therapy Academic Industry Roundtable (STAIR) group guidelines for preclinical evaluation of stroke therapeutics (Liu et al., 2009; Fisher et al., 2009): (1) the vascular recirculation was confirmed by MRA, as an index of the reliability of the ischemic model; (2) silicone rubber coated filaments were used to produce consistent ischemic injuries; (3) standard sized occluder were used depending on the animal strain and size; (4) the temperature was controlled during the ischemic period; (5) this study serves as a pilot study to evaluate putative neuroprotective treatment regimen in the future

Transient MCAO was carried out according to published procedures with minor modifications (Koizumi et al., 1986). Briefly, rats were anesthetized with isoflurane (4–5% induction, 2–2.5% maintenance) in O_2/N_2 (30/70) administered via a face mask. Through a ventral midline neck incision the right common carotid artery (CCA) was exposed up to the bifurcation of internal (ICA) and external carotid artery (ECA) and clamped. The ECA was ligated with a 6–0 silk suture. A silicone rubber coated thread (Doccol Corp. Sharon MA, USA) was introduced into the ECA and advanced into the lumen of the ICA up to a length of 17–18 mm to occlude the MCA. Recirculation was initiated after 1 h by removing the thread and the CCA clamp. Using this procedure, the CCA is reopened and the blood flow to the cerebral hemisphere is re-established. Only vascular branches fed by the ipsilateral ECA remained permanently occluded. The incision wound was finally closed with a 4.0 silk suture and the rat brought back to its home cage.

2.2. Magnetic resonance imaging of different rat strains

Experiments were carried out using Biospec spectrometer (Bruker, Karlsruhe, Germany). The 11.7 T 16 cm bore magnet is equipped with a 9 cm gradient capable of switching 750 mT/m in 90 μs. A 40 mm 1H-resonator was used for RF-transmission and reception.

Animals were anesthetized prior to imaging using 3–4% v/v isoflurane and maintained at 2–2,5% in a gas mixture of O_2/N_2 1:1. The anesthetized rats were placed in sphinx position in a MRI compatible cradle. Rectal temperature was kept at $36 \pm 1\,^{\circ}C$ using heated water blanket and the respiration rate was continuously monitored (MRI compatible animal monitoring system Model 1030, SA Instruments Inc., Stony Brook, NY, USA) to assure the anesthesia depth. Following the automatic calibration (pulse power, shim, and resonance frequency) a high resolution RARE (rapid acquisition with relaxation enhancement) sequence was used with the following parameter: field of view (FOV) 40 mm, image matrix 256×256, 24 slices of 1 mm thickness, pixel resolution 0.156 mm/pixel, either to determine the brain volume in naïve animals or to determine the stroke volume 24 h of 60 min tran-

sient MCAO. No triggering by electrocardiogram or respiration was applied.

2.2.1. Magnetic resonance angiography at 11.7 T

A slab selective 3D-TOF method has been used. To reduce the total imaging time, all 3D data sets were acquired with 75% of the phase encoding steps in the in-plane direction, zero filled to yield the image matrix and isotropic voxel. The parameters of the first set of images were 3 ms echo time (echo at 30% of the readout), a spectral width of 50 kHz and a nominal 45^0 flip angle (1 ms sinc-pulse with 10 lobes) was deployed to excite a 32 mm slab. The image matrix was 256*256*256 and the field of view (FOV) = 32*32*32 mm. The repetition time (TR) was fixed at 30 ms. Using the olfactory bulb as a reference, 6 different MRA data sets were acquired, with the center of the slab was varied in steps of 5 mm from the rostral (10 mm) to the caudal part (−15 mm Bregma) of the brain.

In a second step of optimization a 2.55 ms TE with the echo at 30% of the readout, a nominal 30° flip angle (1 ms gauss), 256*256*256 image matrix, a 32*32*32 mm FOV with one 32 mm slab; TR ranged from 7.51 (shortest time available with a spectral width of 100 kHz), 15, 30 and 60 ms. Ultra high resolution angiograms were acquired with TE = 4.45 ms, TR = 60 ms, 512*512*256 image matrix, a 32*32*16 mm field of view using a 16 mm slab. Two animals of each strain were subjected to the study with the duration of all scans combined not exceeding 4 h. The high resolution protocol was also used to determine high-resolution angiograms 24 h after MCAO for a SD and SHR rat only.

To determine the occurrence of larger cerebro-vascular abnormalities, in 45 SD rats subjected to 60 min MCAO, the following MR protocol was used 24 h after MCAO: TE = 2.55 ms, TR = 15 ms, 128*128*128 image matrix, a 32*32*32 mm field of view using a 32 mm slab. Total imaging time was 184 s (3 min).

2.2.2. Data processing

The contrast to noise ratio (CNR) was determined using Paravison 5.1 by subtraction of the mean signal intensity of a vessel region of interest (ROI) from the background signal intensity of a brain ROI (without apparent blood vessels) derived from within the same slice and dividing it by the standard deviation of the noise. The CNR for the ACA, MCA, the rostral part of the circle of Willis, the ICA as well as for the basilar artery was determined. MR angiograms were obtained in the following way: No data pre-processing, except zero filling, was applied. The raw images were analyzed by ImageJ (Fiji 1.50 h) after rescaling for further processing. Vessels are visualized using maximal intensity projection (MIP) algorithm. Additionally, for comparison, a manual segmentation of brain was performed selectively on the slices of the cranium. The "cleaned" raw images were combined with the slices from outside the cranium and then subjected to MIP to obtain the MR angiograms. This allowed the visualization of the intra-cranial blood vessels as well as the visualization of the connection to the extra-cranial vessels not affected by the pre-processing step. Figs. 1 and 3B were created using Origin (OriginLab, 8Pro).

2.3. Flow-related enhancement considerations

The longitudinal magnetization for a spoiled gradient echo sequence following a number of rf-pulses with the flip angle α is given by (adapted from Bernstein et al., 2004):

$$M_z(t_{n+1}) M_z(t_n) \cos(\alpha) e^{-TR/T_1} + M_0(1 - e^{-TR/T_1}) \quad (1)$$

where $M_z(t_n)$ is the longitudinal magnetization after the n^{th} pulse, with M_0 as the magnetization at equilibrium, T_1 is the longitudinal relaxation time and TR the relaxation time between subsequent excitation pulses.

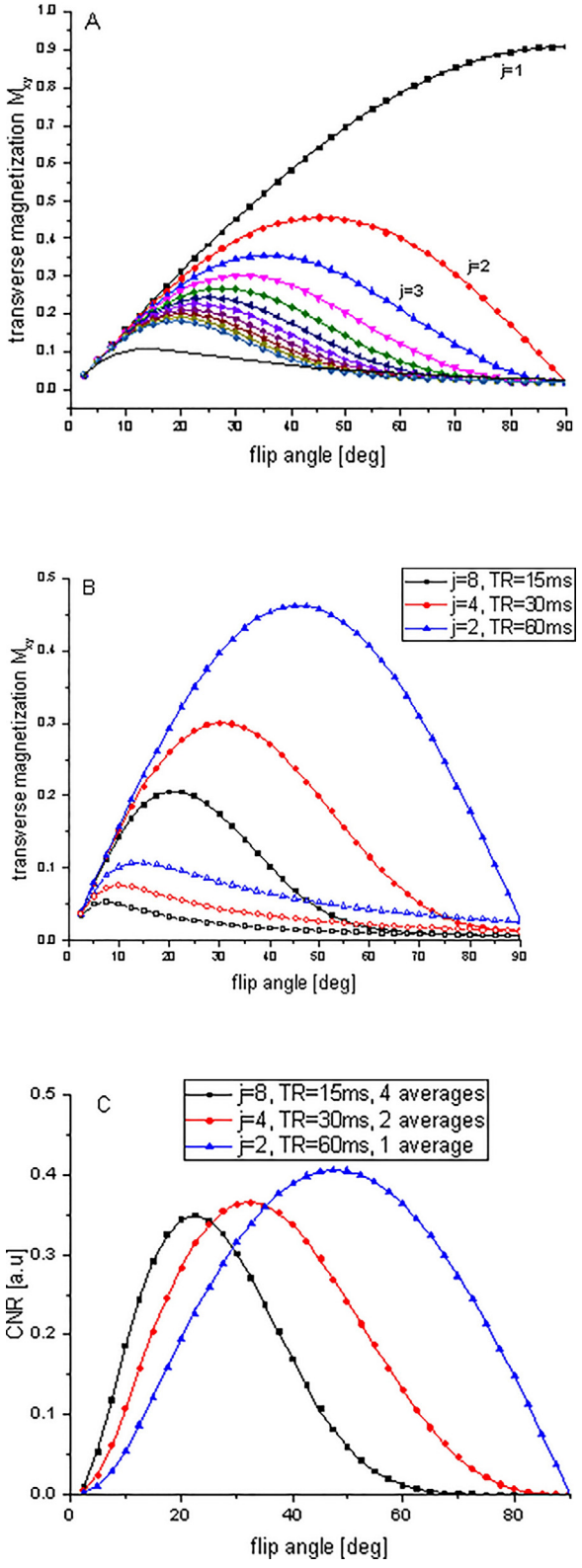

Fig. 1. Plots of A.: normalized transverse magnetization M_{xy} of blood (j = 1–11) and background (solid line) for a TR = 60 ms B.: normalized transverse magnetization M_{xy} of blood (for j = 2, TR = 60 ms; j = 4, TR = 30 ms; j = 8, TR = 15 ms) and with its corresponding background signal from tissue (open symbols) C.: contrast to noise ratio relationship for a constant blood flow velocity and constant total imaging time at different flip angles α.

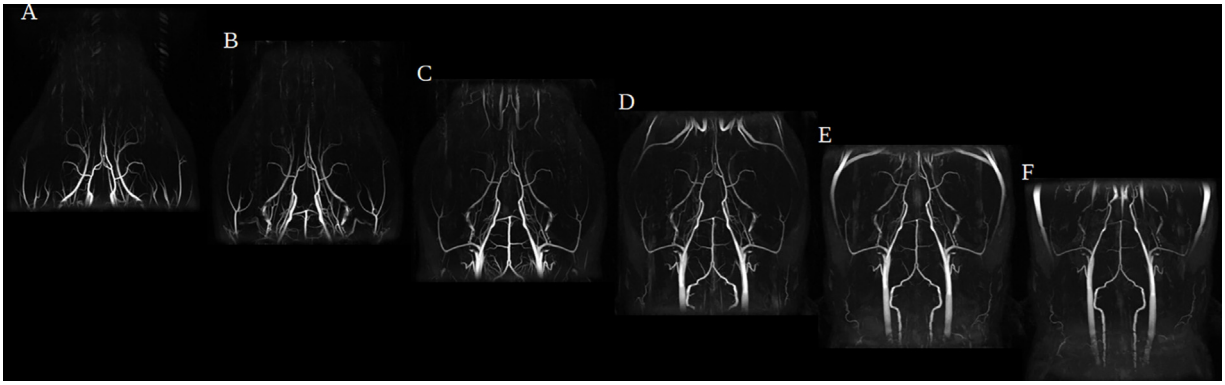

Fig. 2. A–F display the different MR angiograms of the same Sprague Dawley rat from centering the field of view (+10 mm to bregma, A) in steps of 5 mm towards the caudal part (−15 mm bregma, F).

At steady state, with $M_z\,(t_{n+1}) = M_z\,(t_n) = M_{ss}$ is resulting into:

$$M_{ss} = M_0(1 - e^{-TR/T_1})/(1 - \cos(\alpha)e^{-TR/T_1}) \quad (2)$$

The transverse magnetization M_{xy} following the n^{th}- rf-pulse is given as:

$$M_{xy}(TR) = M_{ss}\sin(\alpha)e^{-TE/T_2{}^*} \quad (3)$$

where $T_2{}^*$ denotes the effective transverse relaxation time.

Contrary, the signal (S_j) of the blood in TOF angiography with a spoiled gradient–echo sequence is dependent on j, the number of experienced rf-pulses at a given TR, as well as several imaging parameter (Bernstein et al., 2004; Choi et al., 2015):

$$S_j = M_0\sin(\alpha)[f_{ss} + (\cos(\alpha)e^{-TR/T_1})^{j-1}(1 - f_{ss})]e^{-TE/T_2{}^*} \quad (4)$$

with $f_{ss} = M_{ss}/M_0$.

Fig. 1A displays the normalized signal intensity of the partially saturated magnetization in dependence of the rf-flip angle (in steps of 2.5°). For 11.7 T, a T_1 = 2018 ms and T_2 = 34.7 ms were derived from the average values reported for 9 different rat brain structures of Sprague Dawley rats (de Graaf et al., 2006). For blood, at 11.7 T, the reported T_1 = 2813 ms and T_2 = 46.3 ms values for oxygenated arterial blood at 37 °C were used (Lin et al., 2012). T_2 instead of $T_2{}^*$ was used to calculate the FRE.

The FRE strongly suggests using a high flip angle for vascular structures with high flow velocity or thin slabs, and a lower flip angle for thick slabs and lower velocities. For example, at a TR = 60 ms, for flip angle up to 15°, the contrast to detect the vessel is not optimal, but for up to j = 11, the signal intensity arising from any vessel is similar. Contrary, an optimized flip angle of 60° for a vessel that experiences only two rf-pulses (j = 2) at the given TR, may show substantially higher signal intensity than a vascular structure that experience a higher number of excitation pulses at the same time, and thus, a resulting angiogram would display vessels with substantially different intensity. Therefore, in 3D-TOF that does not aim to image a specific part of a vessel, lower flip angles are a good compromise. Additionally, to reflect that TR directly determines the number of excitation pulses α that any magnetization of blood (arterial or venous) with a constant flow velocity experiences, Fig. 1B compares the FRE of a TR = 60 ms (j = 2) with TR = 30 ms (j = 4) and TR = 15 ms (j = 8). Using this example, the gain in faster imaging time could potentially be used for averaging and to partially offset the contrast dependence on the flip angle (Fig. 1C).

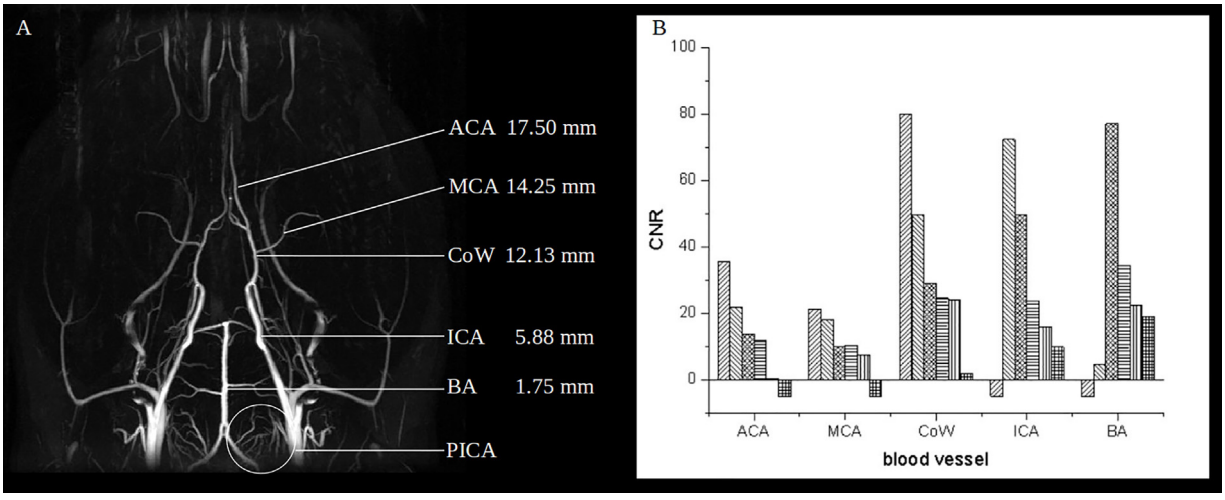

Fig. 3. MR angiogram indicating the posterior internal cerebellar artery (PICA) region (A), as well as the indication for the vessel regions that were analyzed with respect to the isocenter of the magnet and rf-coil (A). For each vessel, six contrast-noise ratioís (CNRs) depending on the center of the field of view (FOV) for the anterior cerebral artery (ACA), the middle cerebral artery branch (MCA), the Circle of Willis (CoW), the internal carotid artery (ICA) as well as the basilar artery (BA) are displayed from left to right for the individual vessel types. Please note the outline of the correct position of the regions, applied to the data set of the six images in Fig. 1A–F. For each vessel, the left column represents the CNR of the most rostral FOV center (10 mm to bregma), the right column the most caudal center below the brain (−15 mm to bregma). A value of minus 5 was assigned if the vessel was outside of the FOV.

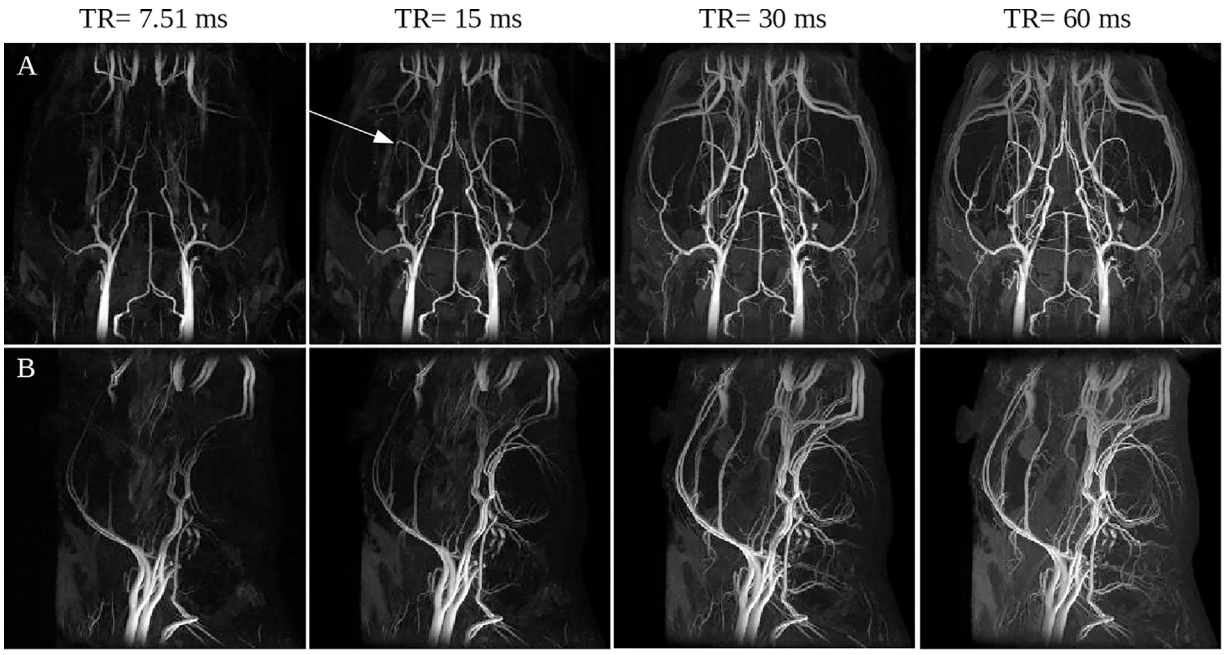

Fig. 4. MR angiograms in Fisher 344 at four different repetition times (TR = 7.51, 15, 30, 60 ms) at an isotropic resolution of 125 μm. The arrow indicates the middle cerebral artery. The total imaging time to acquire the 256^3 matrix ranged from 8.2 to 66 min. Top row: horizontal view, bottom row: sagittal projection.

3. Results

3.1. MR protocol optimization

Fig. 2A–F displays six rat brain angiograms of a Sprague-Dawley rat, obtained by centering the transaxial imaging slab +10 to −15 mm from Bregma. With the FOV centered at 5–10 mm Bregma, the excitation of the front part of the head saturates all venous and arterial structures from the eyes and nose (Fig. 2A, B), in Fig. 2C–F the venous structures are becoming visible in the top of the FOV.

The vertebral arteries are discernable to a large extend (Fig. 2E, F) if the FOV is centered well below the brain. The signal intensity of the basilar artery, measured at the height of the AICA, decreases if the excitation pulse is affecting more and more the vertebral arteries (Fig. 2D–G). From the original images in Fig. 2, the CNR was derived for the ACA (17.5 mm from the isocenter), a MCA branch (14.25 mm), the base of the circle of Willis at around the MCA branching (12.13 mm), the ICA (5.88 mm) as well as the basilar artery (1.75 mm) are indicated in the horizontal angiogram (Fig. 3A). Subsequently, a steady decrease of CNR from 77 to 10 was observed (Fig. 3B) for the ICA if the center of the FOV was placed more and more caudally. Interestingly, the network supplied by the posterior inferior cerebellar artery (PICA), which originate from the vertebral arteries, become only clearly visible if the FOV is adjusted in such a way that the number of excitations of slowly moving blood from the vertebral arteries is minimal (Figs. 2C and 3A). The other two main arteries that supply the cerebellum, the anterior inferior cerebellar artery (AICA) and the superior cerebellar artery (SCA) are also most intense choosing that FOV offset and flip angle. In general, the optimal CNR for any blood vessel could be observed if the vessel of interest is just a few millimeter within the FOV, and thus avoiding to saturate inflowing blood (Fig. 2). It would require an offset of 10 mm to bregma to achieve the highest CNR for the MCA; using this setting, all other main arteries like the cerebellar arteries, the basilar artery and the PCA and ICA would not detected as they are outside of the FOV ((Fig. 2F). Thus, to visualize all main brain arteries, the FOV was centered at bregma as seen in Fig. 3 and the flip angle was reduced to accommodate for the FRE effect.

Fig. 4 displays the rat brain angiograms of a Fisher rat, showing the sagittal and axial views obtained at 4 different repetition times (7.5, 15, 30 and 60 ms), thus increasing inflow delays between excitations. As can be seen with an isotropic resolution of 125 μm, with the increase of total acquisition time from 6 to 50 min, the more distal parts of the MCA supplied vessel structure becomes visible. The extremely fast imaging time of 6 min was not able to reliably identify the branching of the MCA from the circle of Willis as the inflow delay is minimal. Thus, for the subsequent experiments, evaluating the influence of the cerebro-vasculature on the infarct size evolution in 45 animals, a TR of 15 ms was used with lower resolution to be able to acquire a data set in 184 s (3 min).

With an increase in resolution from 125 μm to 62.5 μm, more details, especially larger branches in between the PCA and MCA arising from the circle of Willis or early MCA branches become detectable (Fig. 5A). Given the increased complexity of the MRAs displaying all vessels of the head from within the field of view, we manually segmented the images of all brain slices, set values outside of the skull to zero, and successfully reconstructed the angiograms with an improved signal to noise ratio (Fig. 4B) as noise from outside the head and brighter extracranial structures were removed. We were able to successfully able to identify smaller vessels like the hypothalamic artery (HTA), the anterior choroidal artery (AChA) very clear as well as the initial arterial branches of the peri-amygdoidal complex and to the optical nerve (Fig. 5C and D).

3.2. Visualization of the cerebro-vasculature of different rat strains

All axial angiograms for the six different rat strains are displayed in Fig. 6. As can be seen, all strains have vessels branching of the circle of Willis in between the PCA and MCA, Generally, the SD and SHR strain display a straight transition from the ICA towards the MCA that could potentially explain why these two strains are popular in transient ischemia thread models. Without a significant meaning, we observed abnormal doubling branches from the circle of Willis in the left side of one SD rat, a very small circle in one WK rat (right

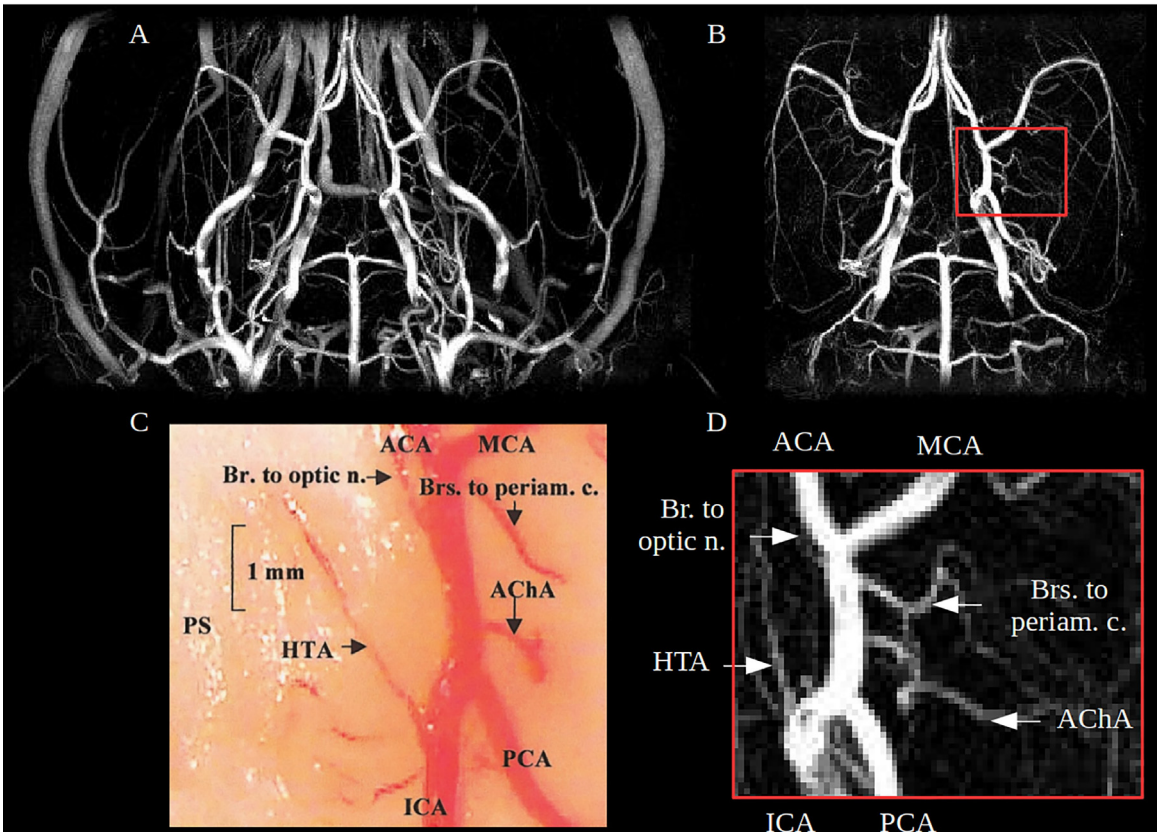

Fig. 5. MR angiogram of the Fisher 344 rat, before (A) and following the removal of the extracranial signal on the height of the cranium (B) prior to applying the maximum intensity projection. The angiogram is acquired within 100 min with an isotropic resolution of 62.5 μm. The post-processing not only simplifies the appearance but allows the direct identifications of the smaller vessels branching from the circle of Willis. The lower two images compare the histological image for vessel identification (C) [reprinted with permission from He et al., 1999] with a zoomed section (D) of the MRA.
Note: Internal carotid artery (ICA), posterior cerebral artery (PCA), middle cerebral artery (MCA) anterior cerebral artery (ACA), hypothalamic artery (HTA), anterior choroidal artery (AChA) arterial branches of the peri-amygdoidal complex (Brs to periam c.) and to the optical nerve (Br. to optical n).

side) and in one LE rat a long parallel vessel additional supplying the MCA territory.

3.3. Frequency of cerebro-vascular abnormalities of the MCA

To investigate the cerebro-vascular abnormality in a larger set of animals, we acquired a 4 min angiogram with a reduced resolution (isotropic 250 μm), 24 h following 60 min transient ischemia (n = 70).

Out of these, 45 animals had an infarct, a MRA examination and survived >24 h, as lethargic animals were euthanatized. The average volume of the infarct size was 192 mm^3 (±119 mm^3) as determined by T2-weighted MRI (see Fig. 7A). Six animals had a "double" MCA (Fig. 6), thus making a single thread MCA occlusion challenging, resulting in an average infarct size of 49 mm^3 (± 52 mm^3). In these animals, the lesions are small and are affecting the hypothalamus as well as internal capsule, indicating an occlusion of the hypothalamic (HTA) and anterior choroidal artery (AChA) (He et al., 1999). If these animal are removed from the previous set of 45, the average infarct size increases to 216 mm^3 (±110 mm^3) with a slightly reduced standard deviation. Ultra-high resolution angiograms 24 h after reperfusion are displayed in Fig. 8A (SD) and B (SHR), demonstrating the complete re-canalization of the MCA as well as of the HTA and AChA. For the SHR rat, the ACA of the affected hemisphere shows no signal intensity.

4. Discussion

The FRE calculation show that in relatively fast flowing blood in vessels like the carotid arteries supply the circle of Willis and the flip angle can be increased to gain sensitivity. On the other hand, all blood vessel that are "uniquely" supplied by the vertebral artery may require a lower flip angle, a longer inflow delay and adjustment in the FOV.

The 40 mm resonator is providing a high SNR with sufficient homogeneity over the sensitive volume, with an increase in T1 at higher field benefits the acquisition of high resolution TOF-MRA. Alternatively, the FRE calculations are still valid for a decoupled coil setup, relying on a homogeneous rf-transmission and thus FRE contrast between stationary tissue and blood remains dependent on the flip angle, TR, slab thickness and flow velocity. However, due to the B1-inhomegeneity of the commonly used brain/surface reception coils, the SNR will vary. Cortical vessels might be detected with an increase of sensitivity, whereby deep lying structures that are "far" away from the reception coil, like vessels arising from the circle of Willis might be more difficult to detect.

Important to note here, as we have used 50% oxygen, 50% nitrogen as the anesthetic carrier gas, hyperoxia is causing vaso-constriction and lowers the cerebral blood flow when compared to breathing room air, (Rostrup et al., 1995; Watson et al., 2000) subsequently resulting in a decrease in T1 and an increase in T2 for brain tissue in rodents (Uematsu et al., 2007). Additionally, oxygenation levels also affect the relaxation times of blood (Lin

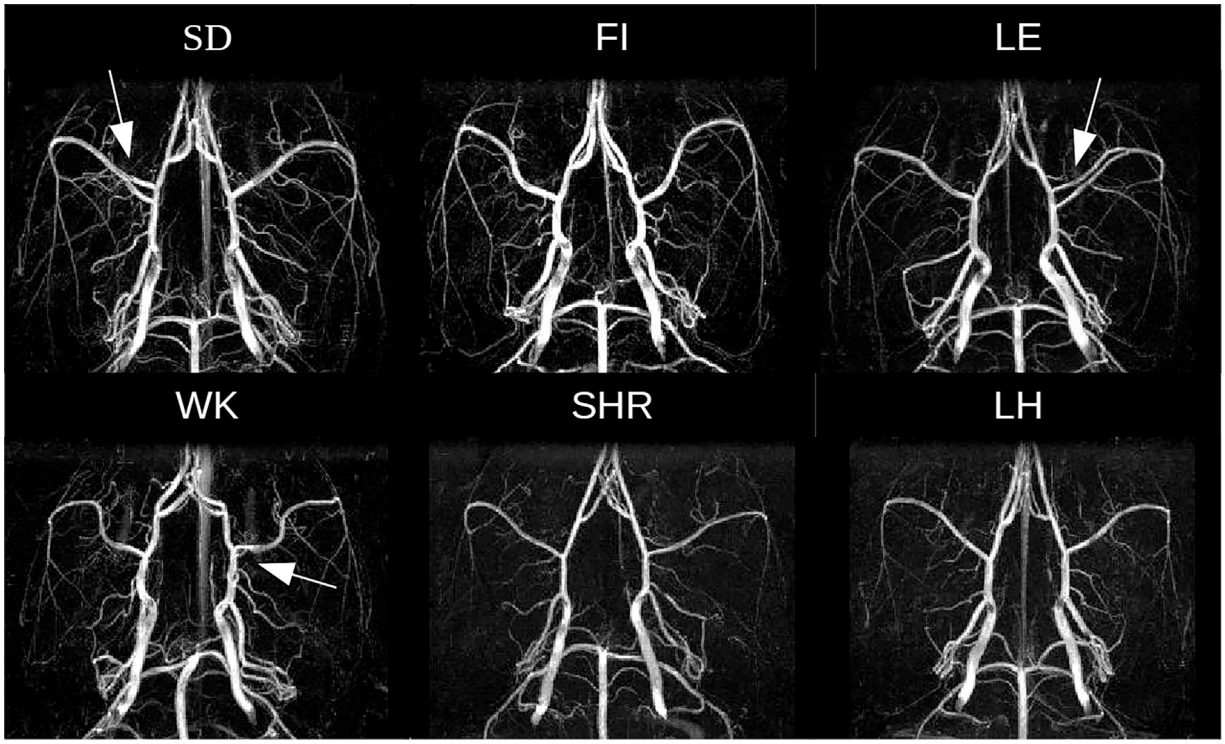

Fig. 6. MR angiograms (MRAs) of six different rat strains: Sprague Dawley (SD), Wistar Kyoto (WK) Spontaneous hypertensive (SHR), Long Evans (LE), Fisher 344 (FI), Lister Hooded (LH). The displayed MRAs, show in detail the anatomy of the cerebro-vascular system. As indicated by the arrows, the LE rat has an abnormal long pair of middle cerebral arteries (MCA) on the right, the WK a close range double branching MCA on the right, and the SD a well separated double branching MCA on the left side.

et al., 2012). The anatomical reference, centering the slice selective MRA acquisition protocol at bregma, is suitable for all rat strains studied. To visualize distal branches of the posterior, anterior and middle cerebral arteries, a nominal flip angle of 30° was chosen (Reese et al., 1999). The dependence of the inflow delay is similar for all rat strains, with the SHR strain potentially require slightly longer repetition times. As vital parameters, like blood pressure and pCO2, were not continuously assessed, this dependence would require detailed examinations in a larger set of animals. To summarize, our high resolution isotropic MRA protocols are optimized to cover a FOV (resolution 125 μm, matrix 256^3, FOV 32 mm) either from the vertebral arteries or with improved resolution and a reduced FOV (resolution 62.5 μm, matrix $512 \times 512 \times 256$, FOV $32 \times 32 \times 16$ mm) starting from roughly the AICA. The larger FOV requires a longer inflow delay (TR = 60 ms) to reliably identify the HTA and AChA with the benefit of also imaging also the larger cerebella arteries in detail. Alternatively, the flip angle might be lowered to accelerate the imaging acquisition. The ultra high resolution images additionally allow the identification of branches to the peri-amydoidal complex and optical nerve, at the expense of an increase in total imaging time from 49 to 98 min. As displayed, the main arteries can be imaged at an isotropic resolution of 200 μm with a flip angle of 30° and a repetition time of 15 ms. Only larger abnormalities, like a well separated double branching of the MCA, can be detected within 3 min. If one is interested in vessels in the cerebellum, the resolution should be increased to at least 100 μm, and the FOV center should be adjusted to accommodate for the FRE of blood flowing into the slab more slowly from the vertebral arteries than from the carotids, as well as anticipating potential reverse flow and vascular spare capacity within the cerebellum itself. Importantly, the protocols rely on a full 3D acquisition of one imaging slab, alternatively multi-slab protocols like MOFTA (multiple overlapping thin-slab acquisition (Parker et al., 1991)) or SLINKY (sliding interleaved k_y (Liu and Rutt, 1998)) shall be considered if larger coverage is required (see also Bernstein et al., 2004, Choi et al., 2012).

Despite the increasing importance of MRA in clinical studies, the method is seldomly used in animal experiments. However, it has been shown when studying the process of arterial occlusive disorders, e.g. in transient ischemia models, that contrast agent administration should be avoided (Reese et al., 1999). It was argued that intra-vascular contrast agents like Gd(DTPA) and super-paramagnetic iron particles might penetrate the brain tissue due to an impaired blood-brain barrier after prolonged ischemia. The accumulation within the brain parenchyma may interfere with supplementary functional and structural MR examinations. As a trend, MRA in rodents is often performed using 2 dimensional multi-slice protocols, resulting in low resolution angiograms, (Gerriets et al., 2004; Chauveau et al., 2011) sufficient to visualize the occlusion side. Hereby, studies exploring the use of MRA in the detection and characterization of models of intra-cerebral aneurysm have been reported for mice (Makino et al., 2015). Contrary, at 11.7 T, as demonstrated here, an increase in field strength shall not only help by a general increase in observable signal, but also offer the opportunity for an improved contrast in TOF-MRA due to an increase in the T1 relaxation times of the stationary signal arising from within the brain. A 3D-TOF sequence was successfully optimized to also identify smaller vessel branching off from the circle of Willis. The center of the FOV can be adjusted to yield the highest CNR for a specific vessel.

Importantly, the “patient” stratification can be done by MRA at 24–48 h, without the use of contrast agent. Roughly 13% of our animals have a “double branched” MCA, which is in general agreement with previously reported values for SD rats (Wang-Fischer, 2009). Naturally, as already highlighted in the introduction, MRA can and is already used to pre-screen the batches of animals that might be subjected to MCAO. The pre-screening protocol has the advantage that outliers can be identified and thus, only animals that

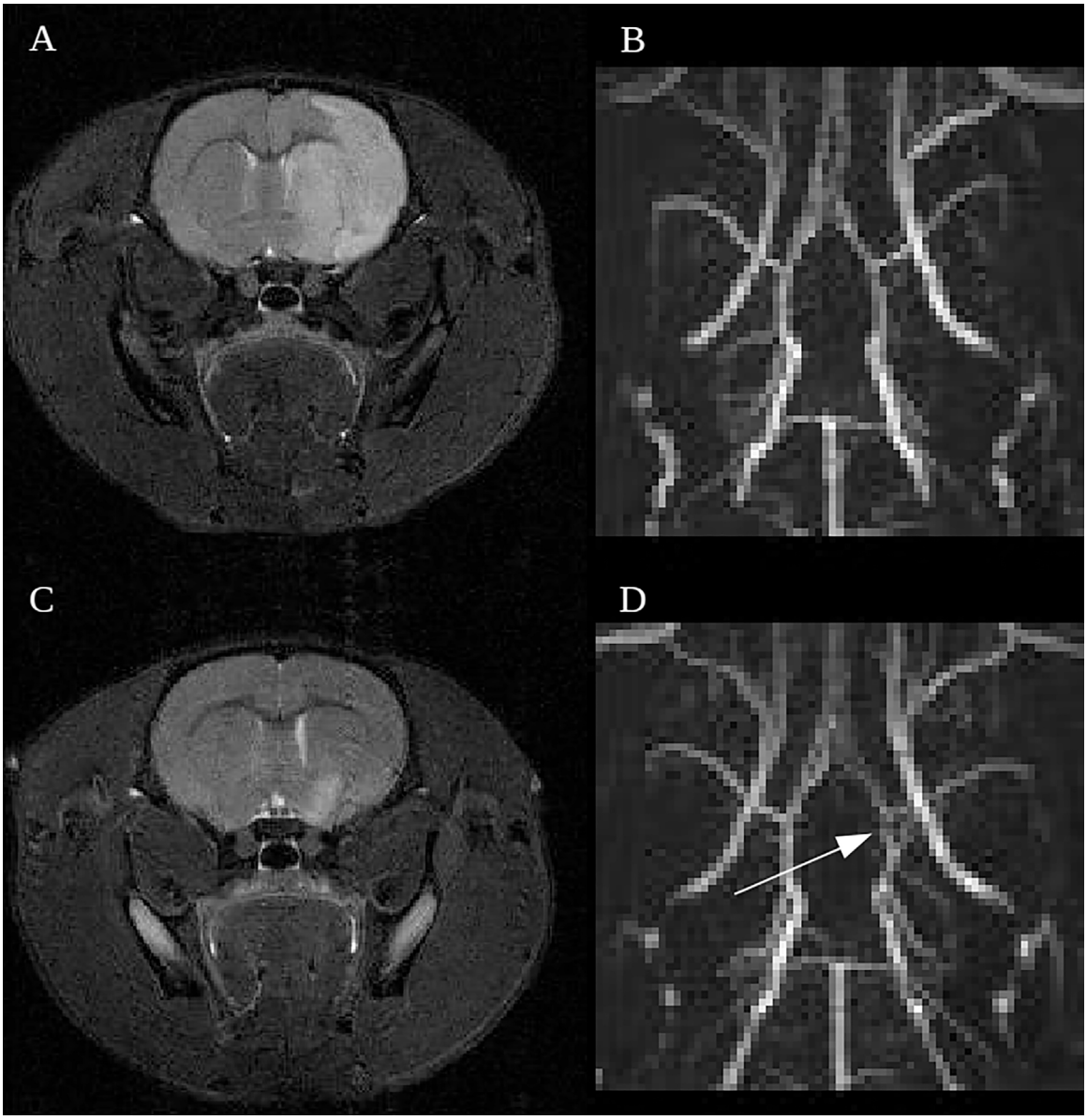

Fig. 7. The top row displays a single slice MR image (A), reflecting a large infarct from an animal with regular MCA as can be seen in the angiogram (B). The bottom row displays a small focal lesion (C) of an animal that had a double MCA (D) as indicated by an arrow.

would meet the inclusion criteria would be subjected to a MCAO. A main disadvantage of protocols that pre-screen animals using MRA is that the study entails an additional session of anesthesia prior to commencing the study. This additional step might increase the complexity of the scheduling, requires an additional imaging session, and may add variability in the outcome and influence additional readout parameter like behavior baseline. Importantly, the execution of MRA at the same time as MR infarct size determination add in our case only an additional 5 min to the imaging session during the sub-acute phase of the disease. If the study is terminated at that point, we have successfully demonstrated the potential to acquire high resolution MRAs on a case by case basis to reveal in detail the cerebro-vascular system and potentially identify compromised reperfusion in a subgroup of animals (Karki et al., 2010)

Depending on the application, imaging times can be reduced to as little as 5 min to detect severe cerebral vessel abnormalities. However, the compromised spatial resolution and short inflow delay does not allow the detection of smaller vessels. Hereby, SD rats, despite having a "double branched" MCA, the CCA occlusion and advancement of the thread caused a small distinct infarct, previously attributed to a failed MCA occlusion (Gerriets et al., 2004) but an obstruction of HTA and AChA (He et al., 1999). Hereby, we might speculate that a larger vessel branching off from the circle of Willis in between the PCA and the MCA that was visualized in the high resolution MRAs might be occluded by the coated thread and thus responsible for the cerebral ischemia in the hypothalamus. Thus, future studies using high resolution MRA may specifically aid longitudinal studies aiming to visualize the HTA, AChA as well as the branching of the periamygdoidal complex and to the optical nerve. Ultimately, MRA has the potential to characterize the vasculature involved, non-invasively and longitudinally, proposed to study temperature regulation in small, deep, non-neocortical infarcts (He et al., 1999).

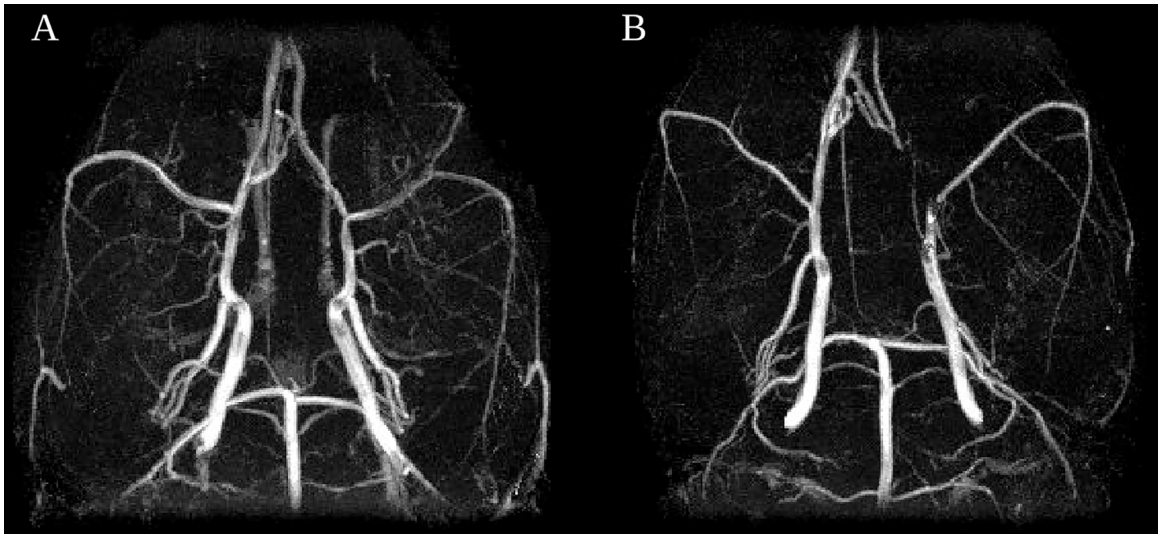

Fig. 8. High resolution angiograms 24 h following a transient MCAO of a SD- (A) and SHR-rat (B) can be obtained despite the presence of a large vasogenic edema.

5. Conclusions

In summary, we have optimized a flow compensated 3D TOF-MRA that can be applied to produce high-resolution angiograms. The method is suitable in at least six different rat strains without using a contrast agent. The visualization of the cerebrovascular system can be enhanced when extra-cranial vessel from the head are removed by a simple post-processing procedure. With a resolution of 62 μm main vessels branching off from the circle of Willis in between the PCA and the MCA could be identified as HTA, AChA and arterial branches supplying the periamygdoidal complex and the optical nerve. Data acquisition time for a 3D TOF-MRA is well below two hours for a high resolution data set, and can be reduced to several minutes when imaging only the principal brain arteries during the same imaging session as usually deployed for infarct size determination 24–48 h following MCAO. The method has been successful in detecting one source of variability in the cerebro-vasculature in SD rats subjected to transient MCAO.

Disclosure/conflict of interest

None of the author has any conflict of interest to declare.

Funding

This work was supported by the Spanish Ministry of Economy and Competitiveness (Project SAF2014-53413-R), the Basque Government (PI_2015_1_53), and Ikerbasque (the Basque Research Foundation).

Authors contribution statement

All authors designed the study and proof-read the final manuscript. GP, PR and TR wrote the initial draft. Data analysis was performed by: GP, MB, PR, TR, SP and DP. MRI experiments were performed by: GP, MJ and TR. All MCAOs were performed by MB.

References

Bardutzky, J., Meng, X., Bouley, J., et al., 2005. Effects of intravenous dimethyl sulfoxide on ischemia evolution in a rat permanent occlusion model. J. Cereb. Blood Flow Metab. 25, 968–977.

Belayev, L., Alonso, O.F., Busto, R., et al., 1996. Middle cerebral artery occlusion in the rat by intraluminal suture: neurological and pathological evaluation of an improved model. Stroke 27, 1616–1622.

Bernstein, M.A., King, K.F., Zhou, X.J., 2004. Handbook of MRI Pulse Sequences. Elsevier/Academic Press, Waltham, MA.

Besselmann, M., Liu, M., Diedenhofen, M., et al., 2001. MR angiographic investigation of transient focal cerebral ischemia in rat. NMR Biomed. 14, 289–296.

de Graaf, R.A., Brown, P.B., McIntyre, S., Nixon, T.W., Behar, K.L., Douglas, L., Rothman, D.L., 2006. High magnetic field water and metabolite proton T1 and T2 relaxation in rat brain in vivo. Magn. Reson. Med. 56, 386–394.

Chauveau, F., Cho, T.H., Perez, M., et al., 2011. Brain-Targeting form of docosahexaenoic acid for experimental stroke treatment: MRI evaluation and anti-oxidant impact. Curr. Neurovasc. Res. 8, 95–102.

Choi, J., Seo, H., Lim, Y., Han, Y., Park, H.W., 2015. Sliding time of flight: sliding time of flight MR angiography using a dynamic image reconstruction method. Magn. Reson. Med. 73, 1177–1183.

Cuccione, E., Padovano, G., Versace, A., et al., 2016. Cerebral collateral circulation in experimental ischemic stroke. Exp. Transl. Stroke Med. 8, 1–9.

Dittmar, M.S., Vatankhah, B., Fehm, N.P., et al., 2006. Fischer-344 rats are unsuitable for the MCAO filament model due to their cerebrovascular anatomy. J. Neurosci. Methods 156, 50–54.

Fisher, M., Feuerstein, G., Howells, D.W., et al., 2009. Update of the stroke therapy academic industry roundtable preclinical recommendations. Stroke 40, 2244–2250.

Fox, G., Gallacher, D., Shevde, S., et al., 1993. Anatomic variation of the middle cerebral artery in the Sprague-Dawley rat. Stroke 24, 2087–2092.

Gao, Y., Goodnough, C.L., Erokwu, B.O., et al., 2014. Arterial spin labeling – fast imaging with steady-state free precession (ASL-FISP): a rapid and quantitative perfusion technique for high field MRI. NMR Biomed. 27, 996–1004.

Gerriets, T., Stolz, E., Walberer, M., et al., 2004. Complications and pitfalls in rat stroke models for middle cerebral artery occlusion: a comparison between the suture and the macrosphere model using magnetic resonance angiography. Stroke 35, 2372–2377.

He, Z., Yamawaki, T., Yang, S., et al., 1999. Experimental model of small deep infarcts involving the hypothalamus in rats: changes in body temperature and postural reflex. Stroke 30, 2743–2745.

Howells, D.W., Porritt, M.J., Rewell, S.S.J., et al., 2010. Different strokes for different folks: the rich diversity of animal models of focal cerebral ischemia. J. Cereb. Blood Flow Metab. 30, 1412–1431.

Karki, K., Knight, R.A., Shen, L.H., et al., 2010. Chronic brain tissue remodeling after stroke in rat: a 1-year multiparametric magnetic resonance imaging study. Brain Res. 1360, 168–176.

Kloiber, O., Miyazawa, T., Hoehn-Berlage, M., et al., 1993. Simultaneous 31P NMR spectroscopy and laser-doppler flowmetry of rat brain during global ischemia and reperfusion. NMR Biomed. 6, 144–152.

Koizumi, J., Yoshida, Y., Nakazawa, T., et al., 1986. Experimental studies of ischemic brain edema, I: a new experimental model of cerebral embolism in rats in which recirculation can be introduced in the ischemic area. Jpn. J. Stroke 8, 1–8.

Lin, A.L., Qin, Q., Zhao, X., Duong, T.Q., 2012. Blood longitudinal (T_1) and transverse (T_2) relaxation time constants at 11.7 Tesla. MAGMA 25, 245–249.

Liu, K., Rutt, B.K., 1998. Sliding interleaved k, (SLINKY) acquisition: a novel 3D MRA technique with suppressed slab boundary artifact. J. Magn. Res. Imaging 8, 903–911.

Liu, S., Zhen, G., Meloni, B.P., et al., 2009. Rodent stroke model guidelines for preclincal stroke trials. J. Exp. Stroke. Transl. Med. 2, 2–27, 1st Edition.

Lythgoe, M.F., Thomas, D., Calamante, F., et al., 2000. Acute changes in MRI diffusion, perfusion, T_1, and T_2 in a rat model of oligemia produced by partial occlusion of the middle cerebral artery. Magn. Reson. Med. 44, 706–712.

Makino, H., Hokamura, K., Natsume, T., et al., 2015. Successful serial imaging of the mouse cerebral arteries using conventional 3-T magnetic resonance imaging. J. Cereb. Blood Flow Metab. 35, 1523–1527.
Mellin, A.F., Cofer, G.P., Smith, B.R., et al., 1994. Three dimensional magnetic resonance microangiography of rat neurovasculature. Magn. Reson. Med. 32, 199–205.
Parker, D.L., Yuan, C., Blatter, D.D., 1991. MR angiography by multiple thin slab 3D acquisition. Magn. Reson. Med. 17, 434–451.
Reese, T., Bochelen, D., Sauter, A., et al., 1999. Magnetic resonance angiography of the rat cerebrovascular system without the use of contrast agents. NMR Biomed. 12, 189–196.
Rostrup, E., Larsson, H.B.W., Toft, P.B., et al., 1995. Signal changes in gradient echo images of human brain induced by hypo- and hyperoxia. NMR Biomed. 8, 41–47.
Sauter, A., Rudin, M., 1995. Strain-dependent drug effects in rat middle cerebral artery occlusion model of stroke. JPET 274, 1008–1013.
Uematsu, H., Takahashi, M., Hatabu, H., et al., 2007. Changes in T1 and T2 observed in brain magnetic resonance imaging with delivery of high concentrations of oxygen. J. Comput. Assist. Tomogr. 31, 662–665.
Wang-Fischer, Y., 2009. Manual of Stroke Models Rats, 1st ed. CRC Press, Boca Raton, p. 18.
Watson, N.A., Beards, S.C., Altaf, N., et al., 2000. The effect of hyperoxia on cerebral blood flow: a study in healthy volunteers using magnetic resonance phase-contrast angiography. Eur. J. Anaesthesiol. 17, 152–159.
Weber, R., Ramos-Cabrer, P., Hoehn, M., 2006. Present status of magnetic resonance imaging and spectroscopy in animal stroke models. J. Cereb. Blood Flow Metab. 26, 591–604.
Yushmanov, V.E., Wang, L., Liachenko, S., et al., 2002. ADC characterization of region-specific response to cerebral perfusion deficit in rats by MRI at 9.4T. Magn. Reson. Med. 47, 562–570.